PAPER

Formation and capture of droplet with high volume ratio of cell to droplet

To cite this article: Zhi Zhao et al 2021 J. Micromech. Microeng. 31 085004

View the article online for updates and enhancements.

You may also like

- An improved pseudopotential multirelaxation-time lattice Boltzmann model for binary droplet collision with large density ratio Wandong Zhao, Ying Zhang and Ben Xu

- Bubble formation in liquid Sn under different plasma loading conditions leading to droplet ejection

W. Ou, F. Brochard and T.W. Morgan

- Motion of generated dumbbell-shaped satellite droplets during liquid dielectrophoresis

Krishnadas Narayanan Nampoothiri and Prosenjit Sen



J. Micromech. Microeng. 31 (2021) 085004 (8pp)

https://doi.org/10.1088/1361-6439/ac0a57

Formation and capture of droplet with high volume ratio of cell to droplet

Zhi Zhao¹, Zhen-Yu Xun¹, Liang-Liang Fan^{1,2,*}, Jiang Zhe³ and Liang Zhao^{4,*}

E-mail: fanllxj@xjtu.edu.cn and lzhao@mail.xjtu.edu.cn

Received 27 October 2020, revised 25 April 2021 Accepted for publication 10 June 2021 Published 28 June 2021



Abstract

High volume ratio of cell to droplet is of great importance for the fast detection on the secreted molecule by rapidly increasing the concentration of the molecule to the detectable level. In this paper, small-volume satellite droplet that encapsulates the cell is continuously generated and captured by a T-shaped microchannel with a branching channel to achieve high volume ratio of cell to droplet. The influence of the flow rate of the continuous phase, the channel geometry and the cell concentration on the formation of the satellite droplet is systematically studied by the experiment. The results show that the smallest satellite droplet with size of \sim 6.5 μ m (\sim 0.14 pl in volume) can be generated at a low cell concentration of 16.7% and an average volume ratio of cell to droplet can be achieved as high as \sim 45.9% (the relative standard deviation is 12.9%). With advantages of continuous manipulation and high volume ratio of cell to droplet, the present method could be potentially utilized as a prerequisite step for the fast detection on the secreted molecule.

Supplementary material for this article is available online

Keywords: droplet formation, satellite droplet, T-shaped microchannel, volume ratio of cell to droplet

(Some figures may appear in colour only in the online journal)

1. Introduction

Microdroplet that encapsulates the cell has great potentials in disease diagnosis, analysis on cellular function and food safety detection [1, 2]. For instance, Klein *et al* encapsulated the cell in the droplet for the high-throughput analysis on the genetic material [3]. An *et al* utilized the droplet for the determination of the food-borne pathogens [4]. Numerous research work have been done to increase the cell encapsulation efficiency [5–7]. For instance, an impressive encapsulation efficiency

from \sim 50% to \sim 90% has been achieved with the help of the trapping-and-encapsulating [8], the inertial ordering [9, 10], the hydrodynamic vortices [11] and the deterministic encapsulation [12]. Although high cell encapsulation efficiency can be achieved, the volume ratio of cell to droplet is typically low. For example, \sim 1.1% volume ratio of cell to droplet was obtained by using the acoustic force and the split of the droplet [13]. Köster *et al* encapsulated a 10 μ m hybridoma cell in a 33 pl droplet, and the volume ratio of cell to droplet was \sim 1.6% [2]. Jing *et al* increased the volume ratio of cell to droplet to be \sim 16.1% by utilizing the jetting microfluidics [14]. Those low volume ratios of cell to droplet are unsuitable for the fast detection on the secreted molecule because it needs

¹ School of Mechanical Engineering, Xi'an Jiaotong University, Xi'an, Shaanxi 710049, People's Republic of China

² School of Food Equipment Engineering and Science (FEES), Xi'an Jiaotong University, Xi'an, People's Republic of China

³ Department of Mechanical Engineering, University of Akron, Akron, OH, United States of America

⁴ State Key Laboratory of Multiphase Flow in Power Engineering, Xi'an Jiaotong University, Xi'an, P. R. China

^{*} Authors to whom any correspondence should be addressed.

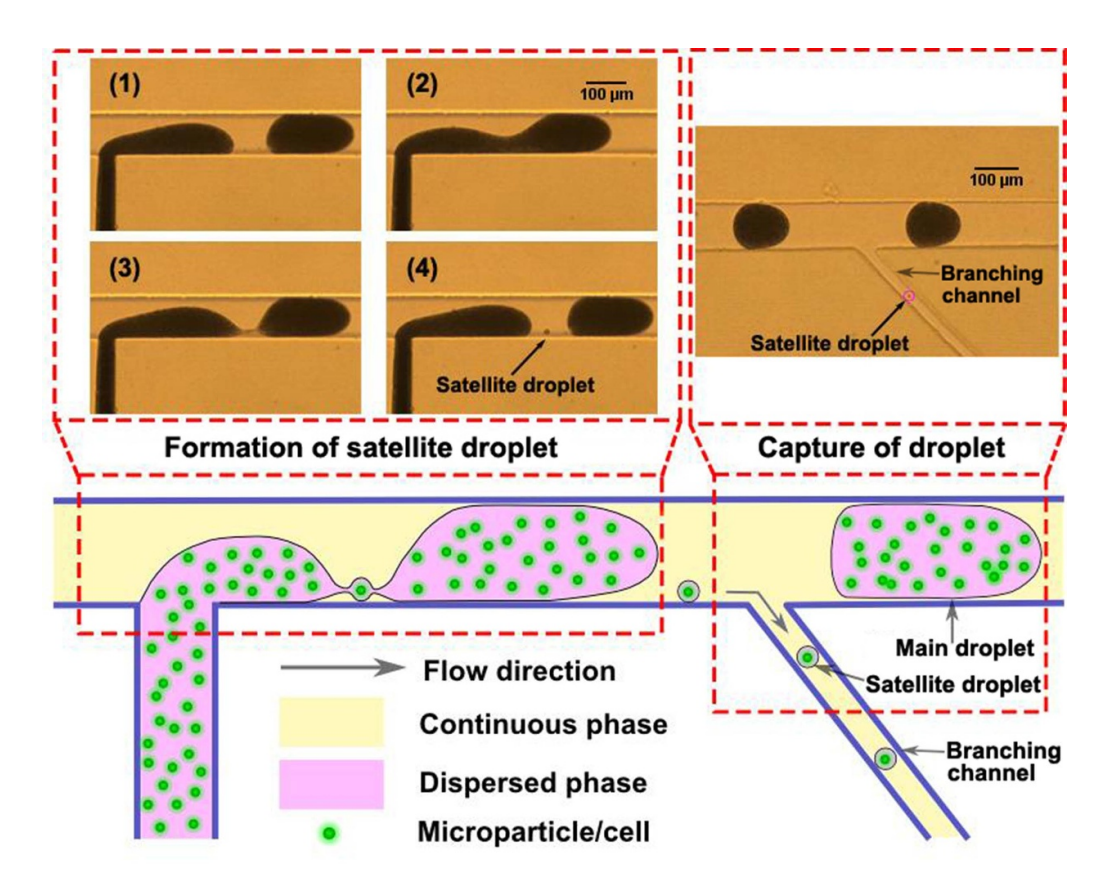


Figure 1. Illustration of the formation and the capture of the satellite droplet that encapsulates the cell.

a long time for the concentration of the molecule to increase to the detectable level [2, 15]. Therefore, the high volume ratio of cell to droplet is required for the fast detection. However, the volume of the droplet reported in the existing literature usually ranged from several to tens of picoliters, which is insufficient to achieve high volume ratio of cell to droplet.

A liquid bridge (neck) often appears in the formation process of the droplet in microchannel because of the viscous stresses and the surface tension [16, 17], and its dimension is influenced by the velocity of the continuous phase fluid and the channel geometry [16]. Could it be utilized to generate the small-volume droplet with high volume ratio of cell to droplet? In the traditional formation process of the droplet, the cell was usually located in the dispersed phase thread [8–12]. We imagine that if the cell was located in the liquid bridge, the breakup process of the interface would be changed and the small-volume satellite droplet that encapsulates the cell might be generated, which would lead to high volume ratio of cell to droplet.

Following the above-mentioned idea, we here report a novel microfluidic method to achieve high volume ratio of cell to droplet where small-volume satellite droplet that encapsulates the cell is continuously generated and captured by a T-shaped microchannel with a branching channel. The influence of the flow rate of the continuous phase, the channel geometry and the cell concentration on the formation of the satellite droplet is systematically studied by the experiment.

2. Channel design and working mechanism

Figure 1 shows the T-shaped microchannel that was used in the experiment. It consisted of a continuous phase channel, a dispersed phase channel and a branching channel. The width of the continuous phase channel (W_c) was 100 μ m. The width of the dispersed phase channel (W_d) was 50, 100 and 150 μ m, respectively. The dimensionless width of the dispersed phase channel $W_{\rm d}{}'$ ($W_{\rm d}{}'=W_{\rm d}/W_{\rm c}$) was used to characterize the channel geometry. The depth of the microchannel was 100 μ m. To capture the satellite droplet, the width of the branching channel was designed to be \sim 35 μ m. Based on the Hagen-Poiseuille equation $(Q_v = \pi \Delta p D_h^4/128 \ \mu l$, where Q_v is the flow rate, Δp is the pressure drop, $D_{\rm h}$ is the hydraulic diameter of the channel, μ is the viscosity of the fluid and l is the length of the channel), it can be obtained that the flow rate ratio of the continuous phase channel to the branching channel is proportional to the fourth power of the hydraulic diameter of the channel. Therefore, in order to capture the 10 μ m satellite droplet, the width of the branching channel should be larger than 31 μ m.

As shown in figure 1, the dispersed phase containing plenty of cells enters the continuous phase channel and obstructs the junction region, which opposes the continuous phase and causes an increase of the hydrodynamic pressure in the continuous phase. Once this hydrodynamic pressure becomes high enough to balance the pressure in the dispersed phase,

the dispersed phase thread will be squeezed and a liquid bridge will be formed. At high cell concentration, the cell will exist in the liquid bridge, and the interface will break up at the two sides of the cell, resulting in the generation of the small-volume satellite droplet that encapsulates the cell. The satellite droplet will become spherical because of the surface tension. We anticipate that the generation of the satellite droplet would be reproducible as long as the cell exists in the liquid bridge. As a result, high volume ratio of cell to droplet would be achieved due to the very small volume of the satellite droplet. Following the hydrodynamic principle, the small satellite droplet would move close to the channel wall and then enter the branching channel (shown in figure 1), eventually achieving the continuous formation and capture of the droplet with high volume ratio of cell to droplet.

3. Experimental section

3.1. Device fabrication

The microchannel was fabricated with the standard soft lithography techniques. SU8-2075 photoresist (MicroChem Inc., USA) was firstly spin coated on a 4-inch silicon wafer with a thickness of $100~\mu m$. Then, photolithography was applied to the SU8 layer to form the mold. Polydimethylsiloxane with the weight ratio of 10:1 (PDMS, Sylgard 184, DowCorning, USA) was poured over the mold, degassed, and cured (65 °C, 2 h), to transfer the patterns onto the PDMS layer. Next, another PDMS layer was made with the weight ratio of 20:1. Finally, the two PDMS layers were bonded at the temperature of 75 °C for 2 h with the thermal diffusion bonding method [18].

3.2. Sample preparation

In the experiment, silicone oil (Sinopharm chemical Reagent, China) was used as the continuous phase liquid. A mixture of the deionized (DI) water and the glycerin (Sinopharm chemical Reagent, China) was utilized as the dispersed phase liquid. To avoid the sedimentation of the cell, the density of the dispersed phase liquid was equal to that of the yeast cell (Angel yeast Co., Ltd, China). The weight ratio of the DI water to the glycerin was about 11:16. The diameter of the yeast cell ranged from 2.5 to 6.0 μ m. Different solid concentrations (C_e) of the yeast cell including 16.7 wt% (\sim 3.2 \times 10⁶ cells μ l⁻¹), 30 wt% (\sim 5.8 \times 10⁶ cells μ l⁻¹) and 66.7 wt% (\sim 1.29 \times 107 cells μ l⁻¹) were prepared in the experiment, respectively.

3.3. Experimental setup

The continuous phase and the dispersed phase were injected into the microchannel by two syringe pumps (KDS 200; KD Scientific Inc., USA) equipped with 5 ml syringes. The flow rates of the continuous phase (Q_c) and the dispersed phase (Q_d) were changed from 400 to 1200 μ l h⁻¹. Poly tetra fluoroethylene tube was utilized to connect the syringe and the channel inlet. Repeated experiments were conducted using multiple devices and the images were captured by an optical microscope (Leica DM4000B, Leica Microsystems, Germany) and

a high-speed charge coupled device (CCD) camera (Fastcam Mini UX100, Photron Limited, Japan). The frame rate was set as 10 000 fps and the resolution was 1280×480 pixels. The software Adobe Photoshop (Adobe Systems Inc. USA) was utilized to measure the size of the droplet, the number of the droplet and the length of the liquid bridge. To clearly show the position of the droplet, a purple circle was added around the satellite droplet.

4. Results and discussion

4.1. The influence of the flow rate of the continuous phase

The formation of the satellite droplet at various flow rates of the continuous phase is shown in figure 2(a). Spherical-shaped satellite droplet that encapsulated the yeast cell was generated and it moved close to the side wall of the microchannel. In the formation process of the main droplet, the cell existed in the liquid bridge, and the interface broke up at the two sides of the cell because of the high hydrodynamic pressure in the continuous phase. Under the influence of the surface tension, the interface shrank to the spherical droplet, and the cell was trapped inside the satellite droplet.

The size and the generation probability of the satellite droplet at various flow rates of the continuous phase are shown in figures 2(b) and (c). The dimensionless droplet length L_s $(L_s' = L_s/W_c$, where L_s is the length of the droplet, W_c is the width of the continuous phase channel) was utilized to characterize the size of the satellite droplet, and the generation probability f_s ($f_s = n_s/n_t$, where n_s is the number of the satellite droplet and n_t is the total number of the interface breakup) was used to characterize the generation possibility of the satellite droplet. It shows that the size and the generation probability of the satellite droplet increased when the flow rate of the continuous phase was changed from 600 to 1000 μ l h⁻¹ (shown in figures 2(b) and (c)). Figure 2(d) shows the dependence of the dimensionless length of the liquid bridge L_n' on the flow rate of the continuous phase $(L_n)'$ was defined as the length of the liquid bridge L_n divided by the width of the continuous phase channel W_c). The length of the liquid bridge increased when the flow rate of the continuous phase was increased from 600 to 1000 μ l h⁻¹. Du *et al* also found that the length of the liquid bridge grew with the increasing flow rate of the continuous phase [17], which might be caused by the increase of the drag effect of the continuous phase on the dispersed phase thread. At higher flow rate of the continuous phase, the liquid bridge became longer, and thus it would contain more liquid and cell. As a result, larger satellite droplet would be generated at higher flow rate of the continuous phase. In addition, it is more likely for the cell to exist in the longer liquid bridge. Therefore, the generation probability of the satellite droplet would become higher when the flow rate of the continuous phase was increased from 600 to 1000 μ l h⁻¹.

4.2. The influence of the channel geometry

The formation of the satellite droplet in the microchannel with different geometries is shown in figures 3(a)–(c). The

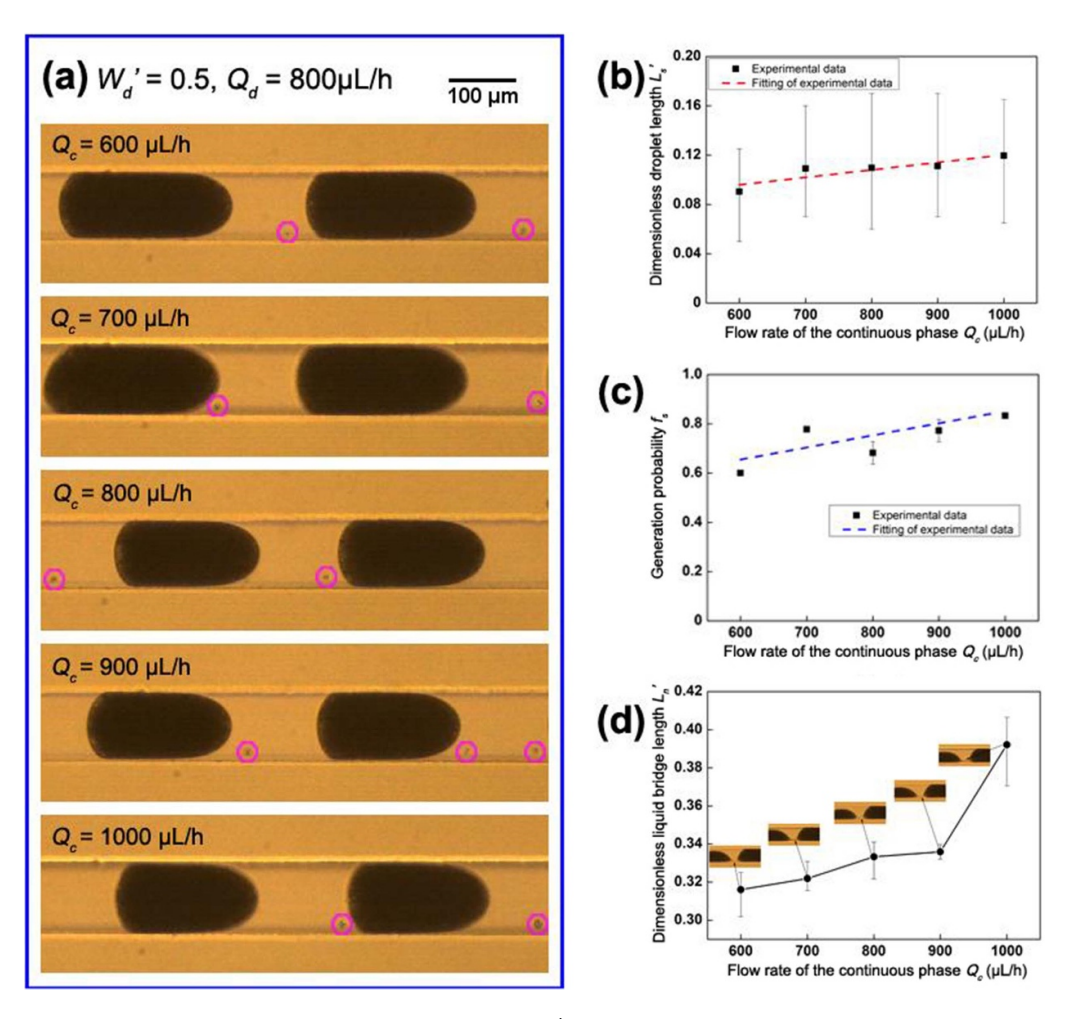


Figure 2. (a) Formation of the satellite droplet in the microchannel ($W_d' = 0.5$) at various flow rates of the continuous phase from 600 to 1000 μ l h⁻¹; (b)–(d) dependence of the size of the satellite droplet, the generation probability of the satellite droplet and the length of the liquid bridge on the flow rate of the continuous phase, respectively.

size of the satellite droplet increased with the increase of the width of the dispersed phase channel while it was almost independent on the flow rate of the dispersed phase (shown in figure 3(e)). The generation probabilities of the satellite droplet at $W_d' = 1.0$ and 1.5 were higher than that at $W_d' = 0.5$ at most tested flow rates of the dispersed phase (shown in figure 3(f)). The length of the liquid bridge increased when the dimensionless width of the dispersed phase channel was changed from 0.5 to 1.5 (shown in figure 3(g)). Therefore, larger satellite droplet and higher generation probability of the satellite droplet would be obtained because of the longer liquid bridge at larger width of the dispersed phase channel. In addition, the generation probabilities of the satellite droplet at $W_{\rm d}' = 1.0$ and 1.5 were almost kept constant while it increased with the flow rate of the dispersed phase at $W_{\rm d}' = 0.5$. It means that in the microchannel with different geometries, there might be a critical liquid bridge length above which the generation probability of the satellite droplet would be kept constant.

The channel geometry greatly influenced the movement of the satellite droplet in the microchannel. When W_d was

0.5 and 1.0, the satellite droplet moved close to the side wall (shown in figures 3(a) and (b)). Following the hydrodynamic principle, these satellite droplets entered the branching channel, and the continuous capture of the satellite droplet could be achieved. However, when W_d was 1.5, large satellite droplets were generated and they periodically migrated in the lateral direction of the microchannel (shown in figure 3(d)). The main droplet moved faster than the satellite droplet when the satellite droplet was generated close to the side wall. Then, because of the different velocities, the satellite droplet was pushed to the center of the channel and moved faster than the main droplet until it met the front main droplet. Next, the satellite droplet was dragged to the side wall by the continuous phase liquid. Finally, the satellite droplet was released from the main droplet and started another periodic migration. The satellite droplet would move away from the side wall in the periodic migration, making it unsuitable for the continuous capture of the satellite droplet. Therefore, the T-shaped microchannel with W_d no more than 1.0 would be more preferred for the continuous formation and capture of the satellite

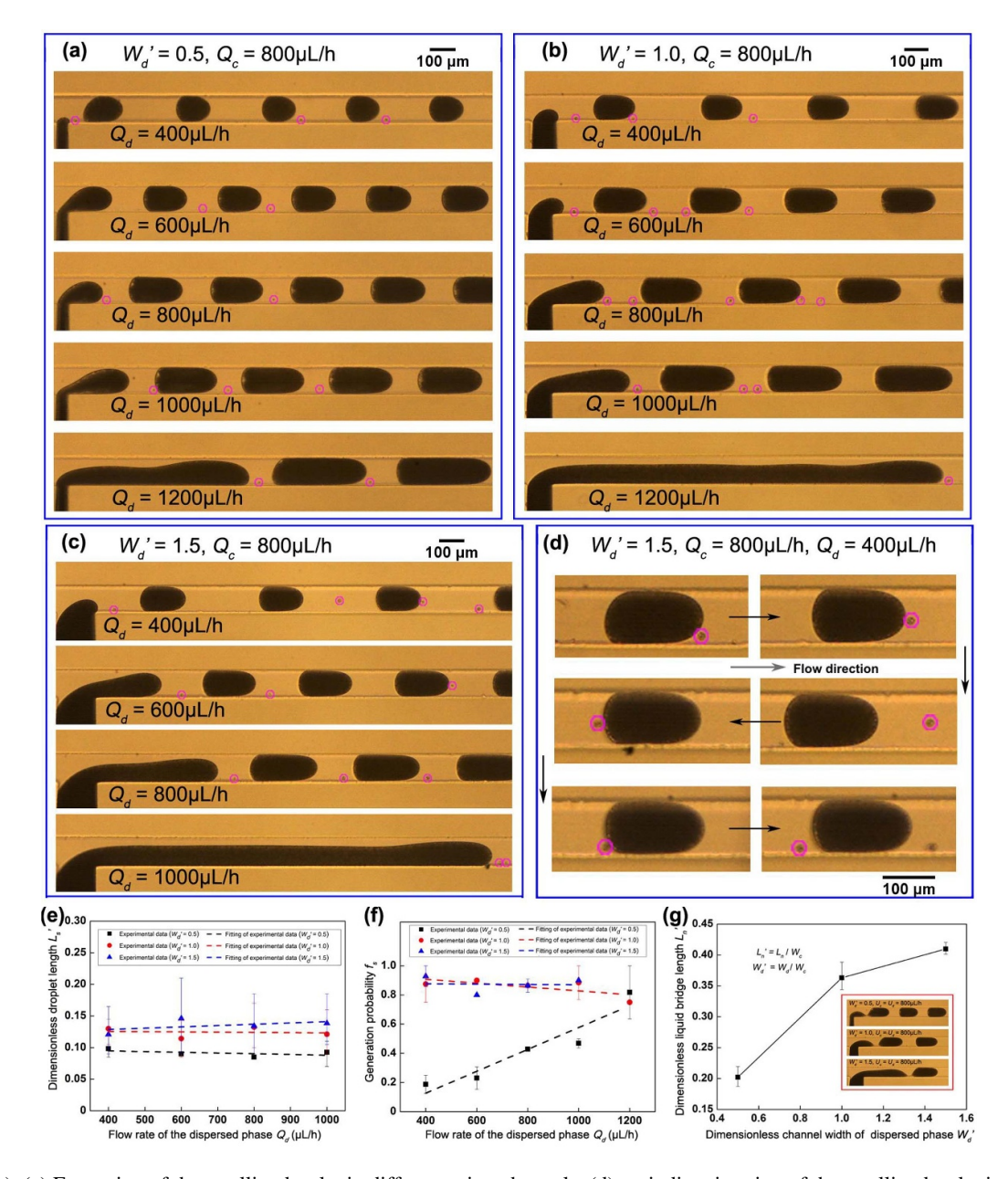


Figure 3. (a)–(c) Formation of the satellite droplet in different microchannels; (d) periodic migration of the satellite droplet in the microchannel at W_d ' = 1.5; (e), (f) The size and the generation probability of the satellite droplet in different microchannels; (g) the length of the liquid bridge in different microchannels ($Q_c = Q_d = 800 \ \mu l \ h^{-1}$).

4.3. The influence of the cell concentration

The formation of the satellite droplet at different cell concentrations is shown in figures 4(a) and (b). It shows that satellite droplets that encapsulated the cell were generated at the cell concentration of 16.7% and 30.0%. The size of the satellite droplet increased when the cell concentration was changed from 16.7% and 66.7% (shown in figure 4(c)). The smallest satellite droplet with size of \sim 6.5 μ m (\sim 0.14 pl in volume) was generated at the low cell concentration of 16.7%. An average volume ratio of cell to droplet could be estimated as \sim 45.9% (relative standard deviation (RSD) = 12.9%), which is much higher than that achieved in other research work and makes it suitable for the rapid detection on the molecule

secreted by the cell. When the cell concentration became high, more cells would exist in the liquid bridge, leading to the generation of large satellite droplet. The generation probability of the satellite droplet was lower at $C_{\rm e}=16.7\%$ than that at $C_{\rm e}=30\%$ and 66.7% (shown in figure 4(d)). In addition, the generation probability of the satellite droplet was kept stable at $C_{\rm e}=16.7\%$ while it increased with the flow rate of the dispersed phase at $C_{\rm e}=30\%$ and 66.7% (shown in figure 4(d)). It might because the probability that the cell existed in the liquid bridged was dominantly determined by the cell concentration when the cell concentration was very low, eventually leading to the low and stable generation probability of the satellite droplet. However, when the cell concentration was high, the cell was more likely to exist in the liquid bridge.

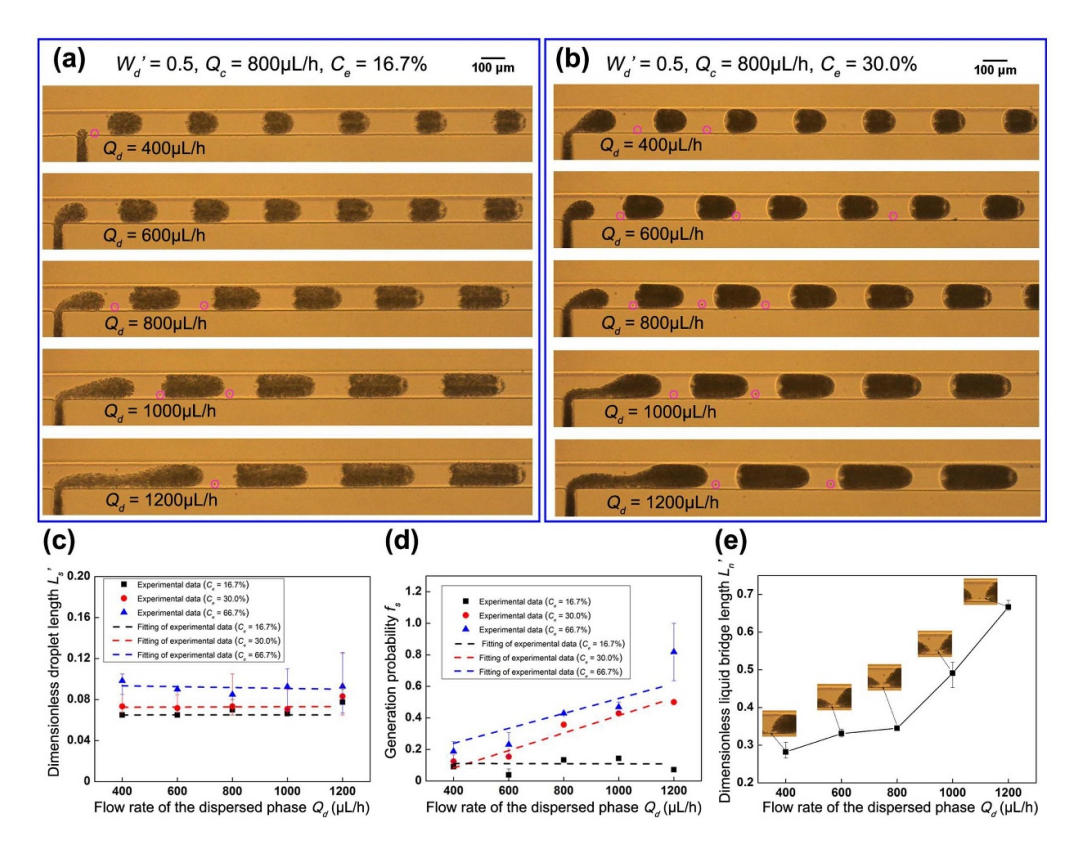


Figure 4. (a), (b) Formation of the satellite droplet at the cell concentration of 16.7% and 30.0%; (c), (d) the size and the generation probability of the satellite droplet at different cell concentrations; (e) the length of the liquid bridge at the cell concentration of 30.0% ($W_d' = 0.5$, $Q_c = 800 \, \mu l \, h^{-1}$).

Table 1. Comparison of the volume ratio of cell/particle to droplet.

Channel geometry	Volume ratio of cell/particle to droplet	Type of the cell/particle	Active/passive	Reference
T-shaped	45.9% (RSD = 12.9%)	Yeast cells	Passive	Present work
T-shaped	13.1%	$10 \mu m$ particle	Passive + active	[7]
T-shaped	1.1%	$5.19 \mu m$ particle	Passive + active	[13]
Flow-focusing	1.6%	Hybridoma cells	Passive	[2]
Flow-focusing	10%	Embryonic stem cells	Passive	[3]
Flow-focusing	12.7%	PC-3 cells	Passive + active	[6]
Flow-focusing	7.9%	HL60 cells	Passive	[9]
Flow-focusing	1.6%	HL60 cells	Passive	[10]
Flow-focusing	6.2% (based on the image)	White blood cells	Passive	[11]
Flow-focusing	0.8% (based on the image)	Mesenchymal stem cells	Passive	[12]
Flow-focusing	16.1%	Cancer cells	Passive	[14]

Meanwhile, the length of the liquid bridge became long with the increase of the flow rate of the dispersed phase (shown in figure 4(e)). As a result, higher generation probability of the satellite droplet was achieved at higher cell concentration. The generation efficiency of the satellite droplet could be further increased by increasing the cell concentration, such as the enrichment of the cell [19]. In addition, an interesting phenomena about the distribution of the cell in the main droplet was obtained in the experiment. At the cell concentration of 16.7% and 30.0%, a tail made up of cells was generated on the main droplet after the interface broke up (shown in figures 4(a) and (b)). Then, the tail moved forwards, and a cell-free region

was induced at the end of the main droplet. Finally, another cell-free region was generated at the head of the main droplet (shown in figures 4(a) and (b)). This interesting phenomena should be induced by the symmetric vortices in the main droplet [20–22].

Continuous formation and capture of the droplet with high volume ratio of cell to droplet was achieved in the present work. Because of the small-volume satellite droplet, the volume ratio of cell to droplet obtained in the present work is higher than that achieved with other methods (shown in table 1), which makes it suitable for lab-chip applications such as act as a prerequisite step for the high-precision biomedical detection. The continuous formation and capture process of the satellite droplet could refer to the supporting video material V1 and V2 (available online at stacks.iop.org/JMM/31/ 085004/mmedia). An expanded structure can be designed at outlet of the microchannel to induce the coalescence of the main droplet so as to recover the lost cell (as shown in supporting video material V3). The viability of the cell that was encapsulated in the satellite droplet was measured with the trypan blue, and the result is shown in the supporting figure S1. It shows that the yeast cell was still alive after passing through the present device. Although high volume ratio of cell to droplet can be achieved with the present method, stable single-cell encapsulation could not be obtained and the size of the satellite droplet was inhomogenous (shown in figures 2(b), 3(e) and 4(c)). Further research work would be conducted in the future to realize the accurate formation of the satellite droplet that encapsulates the cell by precisely manipulating the number and the position of the cell in the liquid bridge.

5. Conclusion

A novel microfluidic method is proposed and tested for the continuous formation and capture of the satellite droplet with high volume ratio of cell to droplet. The experimental results show that the size and the generation probability of the satellite droplet can be controlled by changing the flow rate of the continuous phase, the channel geometry and the cell concentration. The smallest satellite droplet with volume of \sim 0.14 pl was obtained at the cell concentration of 16.7%, and an average volume ratio of cell to droplet could be achieved as high as \sim 45.9% (RSD = 12.9%). In addition, the T-shaped microchannel with $W_{d'}$ larger than 1.0 could not be utilized for the continuous capture of the satellite droplet because of the periodic migration of the droplet. With advantages of continuous manipulation and high volume ratio of cell to droplet, the present method has great potentials in biomedical applications, such as the fast detection on the molecules secreted by the cell.

Data availability statement

All data that support the findings of this study are included within the article (and any supplementary files).

Acknowledgments

This study was supported by the National Natural Science Foundation of China (No. 51706175).

ORCID iDs

Liang-Liang Fan https://orcid.org/0000-0001-9105-9873 Jiang Zhe https://orcid.org/0000-0002-5452-549X

References

- [1] Huang L, Bian S, Cheng Y, Shi G, Liu P, Ye X and Wang W 2017 Microfluidics cell sample preparation for analysis: advances in efficient cell enrichment and precise single cell capture *Biomicrofluidics* 11 011501
- [2] Köster S et al 2008 Drop-based microfluidic devices for encapsulation of single cells Lab Chip 8 1110–5
- [3] Klein A M, Mazutis L, Akartuna I, Tallapragada N, Veres A, Li V, Peshkin L, Weitz D and Kirschner M 2015 Droplet barcoding for single-cell transcriptomics applied to embryonic stem cells Cell 161 1187–201
- [4] An X, Zuo P and Ye B C 2020 A single cell droplet microfluidic system for quantitative determination of food-borne pathogens *Talanta* 209 120571
- [5] Ling S D, Geng Y, Chen A, Du Y and Xu J 2020 Enhanced single-cell encapsulation in microfluidic devices: from droplet generation to single-cell analysis *Biomicrofluidics* 14 061508
- [6] Buryk S, Kieda J and Tsai S 2019 Diamagnetic droplet microfluidics applied to single-cell sorting AIP Adv. 9 075106
- [7] Collins D J, Alan T, Helmerson K and Neild A 2013 Surface acoustic waves for on-demand production of picoliter droplets and particle encapsulation Lab Chip 13 3225–31
- [8] Sauzade M and Brouzes E 2017 Deterministic trapping, encapsulation and retrieval of single-cells *Lab Chip* 17 2186–92
- [9] Edd J F, Di Carlo D, Humphry K J, Köster S, Irimia D, Weitz D A and Toner M 2008 Controlled encapsulation of single-cells into monodisperse picolitre drops *Lab Chip* 8 1262–4
- [10] Kemna E W, Schoeman R M, Wolbers F, Vermes I, Weitz D A and Van Den Berg A 2012 High-yield cell ordering and deterministic cell-in-droplet encapsulation using Dean flow in a curved microchannel *Lab Chip* 12 2881–7
- [11] Kamalakshakurup G and Lee A P 2017 High-efficiency single cell encapsulation and size selective capture of cells in picoliter droplets based on hydrodynamic micro-vortices *Lab Chip* 17 4324–33
- [12] Utech S, Prodanovic R, Mao A S, Ostafe R, Mooney D J and Weitz D A 2015 Microfluidic generation of monodisperse, structurally homogeneous alginate microgels for cell encapsulation and 3D cell culture Adv. Healthcare Mater. 4 1628–33
- [13] Gerlt M S, Haidas D, Ratschat A, Suter P, Dittrich P S and Dual J 2020 Manipulation of single cells inside nanoliter water droplets using acoustic forces *Biomicrofluidics* 14 064112
- [14] Jing T, Ramji R, Warkiani M E, Han J, Lim C T and Chen C H 2015 Jetting microfluidics with size-sorting capability for single-cell protease detection *Biosens. Bioelectron*. 66 19–23
- [15] Guo M T, Rotem A, Heyman J A and Weitz D A 2012 Droplet microfluidics for high-throughput biological assays *Lab Chip* 12 2146–55
- [16] Zhu P and Wang L 2017 Passive and active droplet generation with microfluidics: a review Lab Chip 17 34–75
- [17] Du W, Fu T, Zhu C, Ma Y and Li H Z 2016 Breakup dynamics for high-viscosity droplet formation in a flow-focusing device: symmetrical and asymmetrical ruptures AIChE J. 62 325–37
- [18] Unger M A, Chou H P, Thorsen T, Scherer A and Quake S R 2000 Monolithic microfabricated valves and pumps by multilayer soft lithography Science 288 113–6
- [19] Fan L L, Zhu X L, Yan Q, Zhe J and Zhao L 2019 A passive microfluidic device for continuous microparticle enrichment *Electrophoresis* 40 1000–9

- [20] Li X B, Li F C, Yang J C, Kinoshita H, Oishi M and Oshima M 2012 Study on the mechanism of droplet formation in T-junction microchannel *Chem. Eng. Sci.* 69 340–51
- [21] Malsch D, Kielpinski M, Merthan R, Albert J, Mayer G, Köhler J M, Süße H, Stahl M and Henkel T 2008
- μ -PIV-analysis of Taylor flow in micro channels *Chem. Eng. J.* **135** S166–72 [22] Kinoshita H, Kaneda S, Fujii T and Oshima M 2007
- [22] Kinoshita H, Kaneda S, Fujii T and Oshima M 2007 Three-dimensional measurement and visualization of internal flow of a moving droplet using confocal micro-PIV Lab Chip 7 338–46